

# Changes in biomass burning, wetland extent, or agriculture drive atmospheric NH<sub>3</sub> trends in select African regions

Jonathan E. Hickman<sup>1\*</sup>, Niels Andela<sup>2†</sup>, Enrico Dammers<sup>3</sup>, Lieven Clarisse<sup>4</sup>, Pierre-François Coheur<sup>4</sup>, Martin Van Damme<sup>4</sup>, Courtney Di Vittorio<sup>5</sup>, Money Osohou<sup>6</sup>, Corinne Galy-Lacaux<sup>7</sup>, Kostas Tsigirdis<sup>1,8</sup>, Susanne Bauer<sup>1</sup>

<sup>1</sup>NASA Goddard Institute for Space Studies, New York, USA

<sup>2</sup>NASA Goddard Space Flight Center, Beltsville, USA

<sup>3</sup>TNO, Climate Air and Sustainability, Utrecht, The Netherlands

<sup>4</sup>Université libre de Bruxelles (ULB), Service de Chimie Quantique et Photophysique, Atmospheric Spectroscopy, Brussels, Belgium

<sup>5</sup>Wake Forest University, Winston-Salem, USA

<sup>6</sup>Laboratoire des Sciences de la Matière, de l'Environnement et de l'Energie Solaire, Université Félix Houphouët-Boigny, Abidjan, Côte d'Ivoire

<sup>7</sup>Laboratoire d'Aérodologie, Université Toulouse III Paul Sabatier / CNRS, France

<sup>8</sup>Columbia University, New York, USA

<sup>†</sup>Now at School of Earth and Ocean Sciences, Cardiff University, Cardiff, UK

*\*Correspondence to: jonathan.e.hickman@nasa.gov*

## Abstract

Atmospheric ammonia (NH<sub>3</sub>) is a precursor to fine particulate matter and a source of nitrogen (N) deposition that can adversely affect ecosystem health. The main sources of NH<sub>3</sub>—agriculture and biomass burning—are undergoing or expected to undergo substantial changes in Africa. Although evidence of increasing NH<sub>3</sub> over parts of Africa has been observed, the mechanisms behind these trends are not well understood. Here we use

31 observations of atmospheric NH<sub>3</sub> vertical column densities (VCDs) from the Infrared  
32 Atmospheric Sounding Interferometer (IASI) along with other satellite observations of the  
33 land surface and atmosphere to evaluate how NH<sub>3</sub> concentrations have changed over Africa  
34 from 2008 through 2018, and what has caused those changes. In West Africa NH<sub>3</sub> VCDs are  
35 observed to increase during the late dry season, with increases of over 6% yr<sup>-1</sup> in Nigeria  
36 during February and March (p<0.01). These positive trends are associated with increasing  
37 burned area and CO trends during these months, likely related to agricultural preparation.  
38 Increases are also observed in the Lake Victoria Basin region, where they are associated  
39 with expanding agricultural area. In contrast, NH<sub>3</sub> VCDs declined over the Sudd wetlands  
40 in South Sudan by over 1.5% yr<sup>-1</sup>, though not significantly (p=0.28). Annual maxima in NH<sub>3</sub>  
41 VCDs in South Sudan occur during February through May and are associated with drying of  
42 temporarily flooded wetland soils, which favor emissions of NH<sub>3</sub>. The change in mean NH<sub>3</sub>  
43 VCDs over the Sudd is strongly correlated with variation in wetland extent in the Sudd: in  
44 years when more area remained flooded during the dry season, NH<sub>3</sub> VCDs were lower  
45 (r=0.64, p<0.05). Relationships between biomass burning and NH<sub>3</sub> may be observed when  
46 evaluating national-scale statistics: countries with the highest rates of increasing NH<sub>3</sub> VCDs  
47 also had high rates of growth in CO VCDs; burned area displayed a similar pattern, though  
48 not significantly. Livestock numbers were also higher in countries with intermediate or  
49 high rates of NH<sub>3</sub> VCD growth. Fertilizer use in Africa is currently low but growing;  
50 implementing practices that can limit NH<sub>3</sub> losses from fertilizer as agriculture is intensified  
51 may help mitigate impacts on health and ecosystems.

52

### 53 **1. Introduction:**

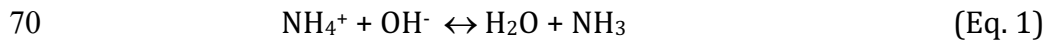
54

55 Ammonia (NH<sub>3</sub>), a reactive nitrogen (N) trace gas, plays a number of important roles  
56 in the atmosphere, with implications for human health, climate, and ecosystems. Once in  
57 the atmosphere, NH<sub>3</sub> contributes to the production of inorganic aerosols, the primary  
58 constituents of fine particulate matter and a serious health hazard (Bauer et al., 2016;  
59 Lelieveld et al., 2015; Pope et al., 2002). NH<sub>3</sub> can also be deposited to downwind  
60 ecosystems, contributing to eutrophication, soil acidification, vegetation damage,  
61 productivity declines, reductions in biodiversity, and indirect greenhouse gas emissions

62 (Denier Van Der Gon and Bleeker, 2005; Krupa, 2003; Matson et al., 1999; Stevens et al.,  
63 2018; Tian and Niu, 2015).

64 Although NH<sub>3</sub> is emitted from natural soils, agriculture is by far the largest source of  
65 NH<sub>3</sub> globally (Behera et al., 2013; Bouwman et al., 1997). Urea fertilizer and livestock  
66 excreta are particularly important substrates for NH<sub>3</sub> formation, and can be volatilized  
67 quickly under favorable environmental conditions (Bouwman et al., 1997). In all soils, NH<sub>3</sub>  
68 is formed in solution following the dissociation of ammonium (NH<sub>4</sub><sup>+</sup>; Eq. 1).

69



71

72 Soil NH<sub>3</sub> production is temperature-dependent, doubling with every 5°C temperature  
73 increase, though the actual soil NH<sub>3</sub> flux is determined in part by plant and soil physiological  
74 and physical factors (Sutton et al., 2013). On average, fertilizer use has been extremely low  
75 in sub-Saharan Africa—often an order of magnitude or more lower than typical in Europe,  
76 the United States, or China (Hazell and Wood, 2008; Vitousek et al., 2009). Livestock manure  
77 N content also tends to be very low in sub-Saharan Africa (Rufino et al., 2006). The low  
78 fertilizer use suggests that natural soils (as opposed to agricultural soils) may be a more  
79 important source in the region than elsewhere in the world. However, agricultural  
80 intensification and increasing fertilizer use has been a central policy focus for many African  
81 countries, with national and regional efforts to increase N inputs by an order of magnitude  
82 or more (AGRA, 2009).

83 After agriculture, biomass burning is the most important source of NH<sub>3</sub> globally  
84 (Bouwman et al., 1997), with roughly 60 to 70% of global NH<sub>3</sub> emissions from fires occurring  
85 in Africa (Cahoon et al., 1992; Whitburn et al., 2015). The amount of NH<sub>3</sub> emitted from  
86 biomass fires is controlled primarily by the type of burning that occurs. N in fuel is present  
87 predominantly in a chemically reduced state, and NH<sub>3</sub> is emitted in greater quantities from  
88 low temperature smoldering combustion in which fuel N is incompletely oxidized (Goode et  
89 al., 1999; Yokelson et al., 2008). Fuel moisture content, which can help determine whether  
90 combustion is smoldering or flaming, is thus an important determinant of biomass burning  
91 NH<sub>3</sub> emissions (Chen et al., 2010).

92 In contrast to other reactive N gases such as NO<sub>x</sub> (nitric oxide + nitrogen dioxide),  
93 NH<sub>3</sub> emissions are typically unregulated outside of Europe (Anker et al., 2018; Kanter,  
94 2018; USDA Agricultural Air Quality Task Force, 2014), and substantial increasing trends  
95 have been observed by the NASA Atmospheric InfraRed Sounder (AIRS) and the Infrared  
96 Atmospheric Sounding Interferometer (IASI) over many of the world's major agricultural  
97 and biomass burning regions during the 21<sup>st</sup> century (Van Damme et al., 2021; Warner et  
98 al., 2017). West Africa has been identified as an important NH<sub>3</sub> source region (Van Damme  
99 et al., 2018), where a trend of increasing NH<sub>3</sub> concentrations in recent decades has been  
100 attributed at least in part to increased fertilizer use (Van Damme et al., 2021; Warner et al.,  
101 2017). Increasing trends have also been observed over central Africa, and attributed to  
102 higher rates of biomass burning (Van Damme et al., 2021; Warner et al., 2017). However,  
103 the studies by Warner et al. (2017) and Van Damme et al. (2021) were global in nature, and  
104 as such could not include detailed explorations of the drivers of trends such as  
105 consideration of emission seasonality or the geographic distribution of emission drivers.  
106 Consideration of these factors is particularly important across large parts of Africa where  
107 both biomass burning and soils are potentially important sources of NH<sub>3</sub> (van der A et al.,  
108 2008).

109 Here we use an eleven-year satellite record to evaluate trends in atmospheric NH<sub>3</sub>  
110 concentrations over Africa from 2008 through 2018, including detailed examination of  
111 three regions where changes are pronounced: West Africa, the Lake Victoria Basin region,  
112 and South Sudan.

113

## 114 **2. Data and Methods**

### 115 **2.1 Global gridded data**

116 Multiple data products were used, including satellite observations and spatial  
117 datasets:

118 -IASI-A, launched aboard the European Space Agency's MetOp-A in 2006, provides  
119 measurements of atmospheric NH<sub>3</sub> and carbon monoxide (CO) twice a day (9:30 in the  
120 morning and evening, Local Solar Time at the equator). Here we use morning observations,  
121 when the thermal contrast is more favorable for retrievals (Clarisse et al., 2009; Van  
122 Damme et al., 2014a). The NH<sub>3</sub> retrieval product used (ANNI-NH<sub>3</sub>-v3R) follows a neural

123 network retrieval approach. We refer to Van Damme et al. (2017) and Van Damme et al.  
124 (2021) for a detailed description of the algorithm. For CO, we used the product obtained  
125 with the FORLI v20140922 retrieval algorithm (Hurtmans et al., 2012). Given the absence  
126 of hourly or even daily observations of NH<sub>3</sub> concentrations in sub-Saharan Africa, the  
127 detection limit of IASI is difficult to determine with certainty. However, the region  
128 experiences high thermal contrast, and IASI seems to be able to reliably observe NH<sub>3</sub> down  
129 to 1 to 2 ppb at the surface (Clarisse et al., 2009; Van Damme et al., 2014b). We gridded the  
130 Level-2 IASI NH<sub>3</sub> and CO products to 0.5° × 0.5° resolution. We used a conventional binning  
131 approach based on the center of each satellite footprint. We did not apply an averaging  
132 weight. Quality control procedures were followed as detailed in van Damme et al. 2017 and  
133 Van Damme et al., 2021. Specifically, the screening of retrievals included filtering of  
134 retrievals where cloud cover is over 10%, where the total column density is below zero and  
135 the absolute value of the hyperspectral range index (HRI) is above 1.5, and where the ratio  
136 of the total column density to HRI is larger than  $1.5 \times 10^{16}$  molecules cm<sup>-2</sup>.

137         The IASI products have been validated using ground-based Fourier transform  
138 infrared (FTIR) observations of NH<sub>3</sub> total columns, with robust correlations at sites with  
139 high NH<sub>3</sub> concentrations, but lower at sites where atmospheric concentrations approach  
140 IASI's detection limits (Dammers et al., 2016; Guo et al., 2021). Compared to the FTIR  
141 observations, total columns from previous IASI NH<sub>3</sub> products (IASI-LUT and IASI-NNv1)  
142 are biased low by ~30% which varies per region depending on the local concentrations.  
143 Although FTIR observations are absent from Africa, earlier work has shown fair agreement  
144 between previous versions of IASI total column densities and surface observations of NH<sub>3</sub>  
145 using passive samplers across the International Network to study Deposition and  
146 Atmospheric chemistry in AFrica (INDAAF) network in West Africa (Van Damme et al.,  
147 2015), including in observations of seasonal variation (Hickman et al., 2018; Ossouhou et al.,  
148 2019). Validation of the IASI CO product using surface, aircraft, and satellite observations  
149 have found total columns to have an error that is generally below 10-15% in the tropics  
150 and mid-latitudes (George et al., 2009; Kerzenmacher et al., 2012; Pommier et al., 2010; De  
151 Wachter et al., 2012). The IASI NH<sub>3</sub> and CO products were used for the years 2008—the  
152 first full year of data available—to the end of 2018. Random errors in observations can be

153 assumed to cancel out in the annual mean, which is what we used in our analysis. With the  
154 assumption that random errors cancel out, only systematic errors related to tropospheric  
155 vertical column contents remain; these systematic errors do not contribute to uncertainty  
156 in trend analyses. In addition, we first take monthly averages based on all daily  
157 observations within a given month before calculating seasonal means to minimize any  
158 potential effects of temporal variability in cloud cover.

159 -The Tropical Rainfall Measuring Mission (TRMM) daily precipitation product (3B42)  
160 is based on a combination of TRMM observations, geo-synchronous infrared observations,  
161 and rain gauge observations (Huffman et al., 2007). Independent rain gauge observations  
162 from West Africa have been used to validate the product, with no indication of bias in the  
163 product (Nicholson et al., 2003).

164 - NOAA Global Surface Temperature Dataset, a 0.5° gridded 2m monthly land surface  
165 temperature product (Fan and van den Dool, 2008). The data set is based on a combination  
166 of station observations from the Global Historical Climatology Network version 2 and the  
167 Climate Anomaly Monitoring System (GHCN\_CAMS), and uses an anomaly interpolation  
168 approach which relies on observation-based reanalysis data to derive spatio-temporal  
169 variation in temperature lapse rates for topographic temperature adjustment.

170 - 500m MCD64A1 collection 6 Moderate Resolution Imaging Spectroradiometer  
171 (MODIS) burned area product for the period 2008-2018 (Giglio et al., 2018). The burned  
172 area data are aggregated by month and gridded to 0.25° resolution, and do not include  
173 burned area from small fires.

174 - MODIS MCD12C1 (collection 5) land cover product, which provides the percentage  
175 of cropped area in each 0.25° grid cell (Friedl et al., 2002). In Africa, agriculture is often  
176 practiced in complex mosaics of agricultural and natural land cover, so we used both the crop  
177 and crop/natural area mosaic MODIS classifications as agricultural area in our analysis.

178 -We also used data on the spatio-temporal distribution of armed conflict events from  
179 the Armed Conflict Location & Event Data Project (ACLED; Raleigh et al., 2010). We included  
180 data for both violent and non-violent conflict events over the period 2008-2018.

181           **2.2 Sudd wetland extent**

182           Monthly flooded area extents of the Sudd Wetland, South Sudan from 2000 to 2017  
183 were derived from 8-day composite MODIS land surface reflectance imagery (MOD09A1);  
184 data from 2005 through 2017 were used in the analyses. We refer to Di Vittorio and  
185 Georgakakos (2018) for a detailed description of the classification procedure designed to  
186 retrieve these data. In summary, monthly flood maps were obtained through a two-stage  
187 classification procedure. The first stage used the full 18-year data set to produce a wetland  
188 land cover map that distinguishes between wetland vegetation classes and their flooding  
189 regimes (permanently flooded, seasonally flooded, or non-flooded). The second stage  
190 compares seasonally flooded pixels from each vegetation class to their non-flooded  
191 counterparts on a monthly basis to identify the timing and duration of flooding for each pixel.  
192 These data were originally derived to calibrate a hydrologic model of the Sudd that is  
193 dependent on Nile flows; therefore, a connectivity algorithm was applied to ensure that all  
194 flooded pixels were physically connected to the Nile River. A few adjustments have been  
195 made to the previously published dataset for the application of this study. The classification  
196 algorithm has been improved to more accurately capture the inter-annual fluctuations in the  
197 permanently flooded areas. The dataset was also extended through 2017, and the total  
198 flooded area was quantified prior to applying the connectivity algorithm. The magnitudes of  
199 the monthly flooded area estimates are now substantially larger because they include areas  
200 flooded from local runoff in addition to areas flooded by the Nile River.

201

202           **2.3 Spatial and national analyses**

203           We evaluated spatial relationships between mean annual tropospheric NH<sub>3</sub>  
204 concentration and several independent variables at 0.25° resolution: population density,  
205 livestock density, and cropped area. Population density and livestock density data are not  
206 available as time series suitable for trend analysis, so we use single year values in our  
207 analyses. We calculated population density based on the 2017 version of the US  
208 Department of Energy’s Gridded Landscan population dataset (Dobson et al., 2000;

209 available at <https://landscan.ornl.gov>). Livestock density was based on the FAO global  
210 gridded livestock dataset for the year 2007 (Robinson et al., 2014). Before analysis, we  
211 converted the livestock densities of chickens, goats, pigs, and sheep to tropical livestock  
212 units (TLU), using values of 0.01, 0.1, 0.2, and 0.1 TLU, respectively; North African cattle  
213 were converted using a factor of 0.7, whereas sub-Saharan cattle were converted using a  
214 factor of 0.5 (Chilonda and Otte, 2006). For cropped area, we used the MODIS MCD12C1  
215 (collection 5) land cover product as described above. We conducted spatial analyses by  
216 establishing a map of 3° grid cells and calculating the correlation between the value of each  
217 independent variable and NH<sub>3</sub> for all 0.5° grid cells within the larger grid cells (N = 36  
218 including water grid cells, though these were excluded from the analysis).

219

220 National data on annual livestock numbers, crop production, and fertilizer N use were  
221 obtained from the UN Food and Agriculture Organization FAOSTAT for 51 African countries  
222 (FAO, 2020). Livestock data consisting of sheep, goats, cattle, and pigs were converted to  
223 tropical livestock units as described above, and buffaloes were converted using a conversion  
224 factors of 0.7 (Chilonda and Otte, 2006). National emissions of CO<sub>2</sub> were obtained from  
225 World Bank Open Data (World Bank, 2019). National-level mean annual cropland area,  
226 burned area, and atmospheric NH<sub>3</sub> and CO concentrations were also calculated for each of  
227 the 51 countries from the spatial datasets described above. Countries were sorted into three  
228 bins based on whether their relative change in mean annual NH<sub>3</sub> concentration was low,  
229 medium or high, and means and standard errors were calculated for each of the three 17-  
230 country bins.

231 Linear trend analyses were conducted using linregress from the scipy.stats package  
232 in Python v3.6.3. Statistical analyses of national scale data were conducted using ANOVA in  
233 R. Data were log or rank transformed when necessary to meet the assumptions of ANOVA.  
234 Values of  $\alpha$  for treatment comparisons following significant ANOVA results were corrected  
235 for multiple testing using Benjamini-Hochberg corrections.

236

237

238 **3. Results & Discussion**



### 239 3.1 Continental distributions and trends

240 Mean annual NH<sub>3</sub> concentrations for 2008-2018 are highest across the savannas  
241 and forest-savanna mosaics in North equatorial Africa, and especially in West Africa; there  
242 are smaller regional hotspots in the Lake Victoria Basin region, South Sudanese wetlands,  
243 and along the Nile delta and river (Fig. 1a). Parts of these regions experience substantial  
244 biomass burning (Fig. 1e), high livestock densities (Fig. 1g), and/or high cropland cover  
245 (Fig. 1h), all of which can contribute to NH<sub>3</sub> emissions. The high concentrations in West  
246 Africa, which is one of the major global NH<sub>3</sub> hotspots (Van Damme et al., 2018), is likely the  
247 result of biomass burning emissions. Biomass burning emissions tend to drive seasonal  
248 variation in NH<sub>3</sub> VCDs in West Africa, with the largest emissions occurring late in the dry  
249 season and early rainy season (Hickman et al., 2021b). In addition to local emissions,  
250 biomass burning emissions and their reactive products are transported to the coast of West  
251 Africa during both the northern hemisphere rainy season, when it is transported from  
252 central and southern Africa, and during the dry season, when it is transported from  
253 biomass burning regions to the east (Sauvage et al., 2007). Most areas with trends are  
254 significant at P=0.2 or higher (Fig. S1).

255 In addition to being hotspots of mean NH<sub>3</sub> concentrations, some of these regions  
256 have also experienced increases in NH<sub>3</sub> concentrations from 2008 to 2018 (Fig. 1b). Like  
257 Warner et al. (2017) and Van Damme et al. (2021), we observed some increases in the  
258 northern grasslands, central African forests, and the Nile region, but we also observe trends  
259 in the Lake Victoria Basin region, which Warner et al. (2017) did not, but Van Damme et al.  
260 (2021) did. Also in contrast to Warner et al. (2017) but in line with Van Damme et al.  
261 (2021), we observe a prominent decline in NH<sub>3</sub> VCDs over South Sudan (Fig. 1b, S1).

262 The Nile region exhibits elevated NH<sub>3</sub> concentrations and a modest positive trend  
263 over the observation period (Fig. 1a, 1b). This trend appears largely to be related to  
264 agriculture and livestock: in a spatial analysis, snapshots of livestock densities and of  
265 population densities are both positively related to changes in NH<sub>3</sub> VCDs (Fig. 2). Although  
266 there is not a positive relationship between agricultural area and NH<sub>3</sub> VCDs over the Nile  
267 region from 2008 to 2018, Egypt's population increased by roughly 25% over that period  
268 (World Bank, 2019), and fertilizer N use increased by roughly 8% after a decline in use

269 between 2004 and 2007 (FAO, 2020), suggesting that increased agricultural N inputs may  
270 be contributing to the trend. We evaluate the other regions in more detail below.

### 271 **3.2 West Africa**

272 The increasing trend in NH<sub>3</sub> VCDs over West Africa are centered over Nigeria and  
273 the southern coast, and to a lesser extent across parts of the wet savanna (Fig. 1b).  
274 Increases in NH<sub>3</sub> VCDs tend to be higher in grid cells with higher population densities in  
275 Nigeria and other parts of West Africa (Fig. 2b), suggesting a possible anthropogenic  
276 influence. The spatial distribution of the mean annual NH<sub>3</sub> trend is overlapped by a  
277 substantial increase in mean annual CO VCDs (Fig. 1b, 1d), pointing to a biomass burning  
278 source, as is also the case in central Africa. Earlier studies have found substantial declines  
279 in annual burned area across the north equatorial African biomass burning region as  
280 detected by MODIS (Andela et al., 2017; Andela and van der Werf, 2014) and related  
281 declines in NO<sub>2</sub> VCDs across the region (Hickman et al., 2021a), which would seem to stand  
282 in contrast to the increasing CO and NH<sub>3</sub> trends observed here.

283 However, the annual decline in burned area and NO<sub>2</sub> VCDs is characterized by  
284 heterogeneity when considering individual months. In West Africa, the dry season is  
285 typically November to February or March. During the transition from the dry to rainy  
286 season in February and March, NO<sub>2</sub> VCDs exhibit increasing rather than decreasing trends  
287 in West Africa, though burned area patterns are not as clear when 2018 is included  
288 (Hickman et al., 2021a; Fig. S2, S3). Although these increases in NO<sub>2</sub> VCDs are small in the  
289 annual context, they occur at a time of year when biomass burning combustion is less  
290 complete, potentially due to greater fuel moisture and declining fire radiative power  
291 (Hickman et al., 2021a; Zheng et al., 2018). These conditions would lead to greater  
292 emissions of less oxidized species such as CO and NH<sub>3</sub>, rather than the more fully oxidized  
293 species such as CO<sub>2</sub> and NO<sub>2</sub> that dominate emissions during the peak of the biomass  
294 burning season (Fig. S2, S4). Indeed, our observations suggest that much of the increasing  
295 NH<sub>3</sub> trend occurs during this transitional period, with NH<sub>3</sub> VCDs increasing by roughly 6%  
296 yr<sup>-1</sup> for all of Nigeria during February and March (Fig. 3, S5; p<0.01). Variation in NH<sub>3</sub> VCDs

297 are positively correlated with CO VCDs (Fig. 4a, S6), which are also increasing during this  
298 period (Fig. 4c, S4).

299 These correlations imply a biomass burning source for the increasing NH<sub>3</sub> VCDs in  
300 West Africa; although the burned area trends are not as clear, it is important to remember  
301 that MODIS undercounts burned area during this time of year by a factor of 3 to 6, and so  
302 would be less sensitive to trends (Ramo et al., 2021; Roteta et al., 2019). Although there is  
303 considerable gas flaring in Nigeria, gas flaring emissions have exhibited long-term negative  
304 trends (Doumbia et al., 2019). In addition, although NO<sub>2</sub> VCDs were found to decrease  
305 across the productive savannas of West Africa, regions of increasing NO<sub>2</sub> VCDs were  
306 observed over large parts of Nigeria, further suggesting that there may be increases—or at  
307 least smaller decreases—in biomass burning in the country (Hickman et al., 2021a). It is  
308 unlikely that changes in chemical sinks—specifically, the formation of nitrate aerosols in  
309 reactions with NO<sub>x</sub> or sulfate—are responsible for the increasing trend: the observed  
310 increase in NO<sub>2</sub> VCDs observed during February and March would be expected to lead to a  
311 shorter NH<sub>3</sub> lifetime and decreasing VCDs. In addition, emissions of SO<sub>2</sub> are relatively low  
312 in West Africa, with moderate emissions occurring in Nigeria, but neither emissions nor  
313 lifetime exhibit clear seasonal variation (Lee et al., 2011).

314 Small agricultural fires are likely an important contributor to the increasing NH<sub>3</sub>  
315 VCDs during the dry-to-rainy season transitional period—a period when agricultural fires  
316 are common in the region (Korontzi et al., 2006). There are large numbers of small fires  
317 that are not detected by MODIS during these months: as noted above, estimates of burned  
318 area during February, March, and April are revised upwards by roughly a factor of 3 to 6  
319 over MODIS when small fires are included (Ramo et al., 2021; Roteta et al., 2019). Many of  
320 these small fires are likely related to agricultural field preparation prior to planting  
321 (Gbadegesin and Olusesi, 1994), which typically takes place in March or April (Vrieling et  
322 al., 2011; Yegbemey et al., 2014). An increase in fires during this transitional period is also  
323 consistent with one of the primary mechanisms behind the overall decline in burned area:  
324 roughly half of the decline is attributed to increased population density and the expansion  
325 of agricultural area, which contributes to the anthropogenic suppression of larger fires  
326 (Andela et al., 2017; Andela and van der Werf, 2014). This agricultural expansion,  
327 however, can be expected to be accompanied by increases in small fires used for the

328 removal of stubble or harvest byproduct (Gbadegesin and Olusesi, 1994), leading to the  
329 increased emissions during the rainy-to-dry season transition observed here.

330 Globally, agricultural emissions from fertilized soils and livestock excreta are the  
331 largest source of  $\text{NH}_3$  (Bauer et al., 2016), and Warner et al. (Warner et al., 2017) suggest  
332 that national-scale changes in fertilizer use could explain the  $\text{NH}_3$  trend over Nigeria.  
333 However, as noted above, much of the increase in West Africa occurs prior to the start of  
334 the planting season—before fertilizer is applied—and appears likely to be due to biomass  
335 burning emissions instead, potentially related to field preparation. Fertilizer or manure  
336 may make a contribution to the increasing trend later in the year, as  $\text{NH}_3$  VCDs increase in  
337 the wet savanna during May, June, and July (Fig. 3), though there are also significant  
338 correlations between  $\text{NH}_3$  and CO VCDs (Fig. 4), suggesting that biomass burning may  
339 continue to play an important role. However, average N fertilizer use in West Africa is  
340 universally under  $40 \text{ kg N ha}^{-1} \text{ yr}^{-1}$ , typically under  $20 \text{ kg N ha}^{-1} \text{ yr}^{-1}$ , and is under  $10 \text{ kg N}$   
341  $\text{ha}^{-1} \text{ yr}^{-1}$  in Nigeria—over an order of magnitude lower than rates in Europe, the United  
342 States, and China (FAO, 2020). Although percentage changes in fertilizer use are  
343 substantial, in absolute terms they represent increases of less than  $2 \text{ kg N ha}^{-1} \text{ yr}^{-1}$ , and  
344 frequently less than  $1 \text{ kg N ha}^{-1} \text{ yr}^{-1}$ , a relatively small but perhaps not entirely trivial  
345 perturbation to the N cycle: Between 2000 and 2007, total N deposition averaged  $8.38 \text{ kg N}$   
346  $\text{ha}^{-1} \text{ yr}^{-1}$  in wet savanna and  $14.75 \text{ kg N ha}^{-1} \text{ yr}^{-1}$  in forest ecosystems based on surface  
347 sampling sites (Galy-Lacaux and Delon, 2014), and biological N fixation in tropical and wet  
348 savannas has been estimated as ranging from  $16$  to  $44 \text{ kg N ha}^{-1} \text{ yr}^{-1}$  (Bustamante et al.,  
349 2006). These estimates suggest that fertilizer increases may represent a 1 to 2% annual  
350 increase in N inputs. But given the small magnitude of fertilizer applications, it appears  
351 unlikely that changes in fertilizer use can explain the entirety of  $\text{NH}_3$  increases during the  
352 growing season. Our analyses do suggest that livestock may contribute to increasing  $\text{NH}_3$   
353 VCDs over the Sahel, from roughly 15 to 18N (Fig. 2a). However, many of these pixels are  
354 also those where population density appears to be playing a role (Figure 2b) and where  
355 correlations between  $\text{NH}_3$  and CO VCDs are present during the transition from the dry to  
356 rainy season (Fig. S7), which may reflect a contribution from agricultural fires.

357

358

### 3.3. South Sudan

359           The most notable declining trend in  $\text{NH}_3$  VCDs occurs in South Sudan over the Sudd  
360 wetlands at a rate of over  $2\% \text{ yr}^{-1}$  (Fig. 1b;  $p=0.20$ ). It appears that this decline is related to  
361 interannual variation in the flooded extent of the Sudd, a vast wetland that connects the  
362 White and Blue Nile tributaries. Seasonal variation of inflow to the Sudd leads to variation  
363 in flooded extent: an area of roughly  $15,000 \text{ km}^2$  is permanently flooded, and another  
364 roughly  $15,000 \text{ km}^2$  is temporarily flooded each year, with considerable interannual  
365 variation in the total flooded area (Di Vittorio and Georgakakos, 2018). Among other  
366 factors, drying soils should increase production and emissions of  $\text{NH}_3$  from soils, as Eq. 1 is  
367 shifted to the right (Clarisse et al., 2019). Earlier work evaluating an  $\text{NH}_3$  hotspot over Lake  
368 Natron in Tanzania found that the drying of seasonally flooded soils leads to large  
369 emissions of  $\text{NH}_3$ : As the waters of Lake Natron recede during the dry season each year  
370 and the surrounding mud flats dry out,  $\text{NH}_3$  VCDs increase rapidly, with hotspots appearing  
371 over the mudflats (Clarisse et al., 2019). These elevated VCDs are attributed to multiple  
372 possible factors, including the effects of drying on concentrations of  $\text{NH}_3$  in solution (which  
373 increases the concentration gradient with the atmosphere), reduced biological uptake of  
374  $\text{NH}_3$ , convective transport of dissolved  $\text{NH}_3$  from depth to the soil surface, and increased  
375 mineralization of labile organic matter (Clarisse et al., 2019).

376           We find the same clear seasonal relationship between wetland flooded extent and  
377  $\text{NH}_3$  concentrations over the Sudd—VCDs increase as waters recede from the temporarily  
378 flooded area, leading to annual maxima from February through May (Fig. 5a; bounding box  
379 of 29E to 31.5E and 6N to 9.9N). Like the entire country, seasonal variation in  $\text{NH}_3$  VCDs  
380 over the Sudd follow variation in surface temperature, but  $\text{NH}_3$  concentrations over the  
381 Sudd are substantially elevated compared to surrounding regions during this time of year  
382 but not others, suggesting that a mechanism in addition to temperature is contributing to  
383 the elevated emissions in the Sudd during February through May, a period that spans the  
384 end of the dry season and start of the rainy season (Fig. S8). This conclusion is supported  
385 by an analysis of interannual variation of VCDs during the February through May period:  
386 Interannual variation in  $\text{NH}_3$  VCDs is largely decoupled from variation in temperature, but

387 NH<sub>3</sub> VCDs appear to vary inversely with the amount of area that dries out each year (Fig.  
388 5b). Over the period for which flooded extent data are currently available for the Sudd, the  
389 minimum flooded extent tends to increase—that is, less area dries out each year—resulting  
390 in an overall decline in NH<sub>3</sub> VCDs. Linear regression reveals that this change in flooded  
391 extent explains a large proportion of the annual variation in NH<sub>3</sub> in the Sudd bounding box  
392 ( $r=-0.64$ ,  $p=0.046$ ), as well as for the country as a whole ( $r=-0.60$ ,  $p=0.065$ ). These analyses  
393 strongly suggest that the declining trend in NH<sub>3</sub> over the Sudd is a direct result of an overall  
394 increase in the minimum flooded extent over the observation period.

395         It is possible that conflict in South Sudan could contribute to the decline in NH<sub>3</sub>  
396 VCDs. In 2013, a civil conflict emerged in South Sudan that was ultimately responsible for  
397 the displacement of millions of people (Global Internal Displacement Monitoring Centre,  
398 2020; World Bank, 2019) and the disruption of livestock migration patterns (Idris, 2018).  
399 However, these disruptions appeared only after the onset of the long-term change in NH<sub>3</sub>,  
400 and appear unlikely to make an important contribution to the observed interannual  
401 variation (SI Text, Fig. S9, S10).

402         It is unlikely that changes in chemical sinks are responsible for the decline in NH<sub>3</sub>  
403 VCDs. VCDs of tropospheric NO<sub>2</sub> are also decreasing in the region (Fig. S11), which is  
404 suggestive of less formation of particulate-phase ammonium rather than more.  
405 Anthropogenic SO<sub>2</sub> emissions in Africa in general and South Sudan in particular are very  
406 low (European Commission Joint Research Centre (JRC)/Netherlands Environmental  
407 Assessment Agency (PBL), 2016), and would not be expected to be emitted from the Sudd;  
408 more generally, the clear spatial association between the NH<sub>3</sub> trend and the Sudd (Fig. 1,  
409 Fig. S12) is strongly suggestive of changes in emissions rather than atmospheric processes  
410 being responsible for the trend.

411

### 412         **3.4 Lake Victoria Basin region**

413           The Lake Victoria Basin and its surroundings—an area including elevated mean NH<sub>3</sub>  
414 VCDs—exhibit an increasing NH<sub>3</sub> trend (Fig. 1b, Fig. 6, Fig. S13), which appears to be the  
415 result of increasing agricultural activity in the area. The region includes a high and  
416 increasing density of agricultural land (Fig. 1h, Fig. 2d, Fig. S14), and these increases in  
417 cropped area are positively correlated with increases in NH<sub>3</sub> VCDs across much of the  
418 region (Fig. 2c). The northern and southern halves of the Lake Victoria region—which  
419 straddles the equator—have distinct growing seasons: in the north, the season generally  
420 starts in April, whereas in the south, it starts in November or December (Vrieling et al.,  
421 2011). Some of the long-term trend reflects this seasonality, with increases in the north  
422 and south occurring during their respective growing seasons (Fig. 3, Fig. S15). Fertilizer  
423 use in the Lake Victoria region is low: national averages range from about 1 to 3 kg  
424 nutrients ha<sup>-1</sup> yr<sup>-1</sup> in Uganda to about 35 to 40 kg nutrients ha<sup>-1</sup> yr<sup>-1</sup> in Kenya (Elrys et al.,  
425 2019; World Bank, 2019); to put these numbers in context, Organization for Economic  
426 Cooperation and Development (OECD) countries use about 135-140 kg nutrients ha<sup>-1</sup> yr<sup>-1</sup>  
427 (World Bank, 2019). Although rates of fertilizer use have increased by substantial  
428 proportions, the absolute amount of increase is relatively small, typically roughly 1 to 10 kg  
429 nutrients decade<sup>-1</sup>. Unlike in West Africa, however, interannual variation in burned area  
430 (Fig. 6, S16) does not exhibit a clear relationship with changes in NH<sub>3</sub> VCDs. Consequently,  
431 we expect that both the expansion and intensification of agriculture in the region  
432 contribute to the increasing NH<sub>3</sub> VCDs.

433           We note that there is a negative correlation between cropland area and NH<sub>3</sub> VCDs in  
434 Uganda, north of Lake Victoria (Figure 6b). We expect this is a consequence of the  
435 extremely low fertilizer use in Uganda (Masso et al., 2017) , which leads to depletion of soil  
436 N—and thus substrate for ammonia volatilization—over time (Cobo et al., 2010).

437           We also note that there is an apparent increase in NH<sub>3</sub> VCDs over the lake itself. It is  
438 important to note that differences in conditions over the lake and adjacent land cover—e.g.,  
439 emissivity, thermal contrast, etc.—contribute to substantial differences in mean retrieved  
440 NH<sub>3</sub> VCDs over the lake relative to the surrounding land surface. Both monthly and  
441 interannual variation in NH<sub>3</sub> VCDs over Lake Victoria correspond closely to variation in

442 NH<sub>3</sub> VCDs over the surrounding land surface (Figure S17, S18), suggesting that the trend  
443 over the lake results from transport of NH<sub>3</sub> emitted from the surrounding land surface.

444

### 445 **3.5 National-scale relationships**

446 Examining relationships at a national scale can provide insight into relationships  
447 between changes in agricultural or biomass burning and changes in atmospheric NH<sub>3</sub> VCDs  
448 at larger scales. When grouping countries into three bins based on their annual percentage  
449 changes in NH<sub>3</sub> VCDs, there is some evidence for a broad relationship between livestock  
450 and NH<sub>3</sub> VCDs at the national scale (Fig. 7). The rate of change in national-scale NH<sub>3</sub> VCDs  
451 varies significantly among bins ( $p < 0.001$ ; rank transformed, though note that residuals  
452 may still deviate from normality). The annual percentage changes in livestock in TLUs vary  
453 significantly by bin ( $p = 0.042$ ; rank transformed), with the middle bin higher than the  
454 bottom bin ( $p = 0.1$ ) and the high bin higher than the bottom bin ( $p = 0.06$ ). Annual  
455 percentage changes in fertilizer N ( $p = 0.58$ ) and crop production ( $p = 0.62$ ; rank  
456 transformed) did not vary by bin.

457

458 Instead of a direct agricultural relationship with changes in NH<sub>3</sub> VCDs, there is the  
459 possibility that changes in biomass burning are associated with changes in NH<sub>3</sub> VCDs.  
460 Although the differences in the annual percentage change in burned area were not  
461 significant among bins ( $p = 0.54$ ; rank transformed), the overall pattern is consistent with  
462 earlier results finding that a reduction in burned area across the northern biomass burning  
463 region was associated in part with the expansion of agriculture and presumed  
464 anthropogenic suppression of fire (Andela et al., 2017; Andela and van der Werf, 2014).  
465 However, burned area as measured by MODIS is likely an imperfect predictor for NH<sub>3</sub>  
466 emissions—as noted previously, MODIS underestimates burned area by a factor of 3 to 6  
467 during shoulder seasons (Roteta et al., 2019), which is when fires are expected to emit  
468 more reduced species such as NH<sub>3</sub> (Zheng et al., 2018). In contrast to burned area, the  
469 annual change in column densities of CO—which tends to be co-emitted with NH<sub>3</sub> from  
470 fires—differed significantly among bins ( $p < 0.001$ ; rank transformed) and was significantly  
471 higher in the high bin than in the low or medium bins ( $p < 0.001$ , post-hoc tests). The higher



472 annual CO changes in the high bin could related to larger anthropogenic fossil fuel  
473 emissions, but we see no difference among bins in growth rates of CO<sub>2</sub> emissions (p=0.48;  
474 Figure S19); such a difference would be expected if differences in economic development  
475 were responsible for the CO differences. These results leave open the possibility that  
476 changes in either biofuel emissions or biomass burning emissions—perhaps from smaller  
477 fires not observed in the MODIS burned area product—may be primarily responsible for  
478 the difference in CO between bins, and may be contributing to the differences in NH<sub>3</sub>  
479 between bins. Changes in NO<sub>2</sub> VCDs and SO<sub>2</sub> concentrations can affect the lifetime of NH<sub>3</sub>  
480 (the latter by changing SO<sub>4</sub> concentrations), but do not appear to make an important  
481 contribution to the observed trends in NH<sub>3</sub> VCDs among bins (Fig. S19, SI text).  
482 Temperature, likewise, does not appear to play an important role (SI text).

483

#### 484 **4. Conclusion**

485 Using IASI, we have observed both increases and decreases in atmospheric NH<sub>3</sub>  
486 VCDs in different regions in Africa between 2008 and 2018, with different factors affecting  
487 trends in different regions.

488 We observed increases in NH<sub>3</sub> VCDs in West Africa, which earlier work had  
489 concluded was likely related to increased fertilizer use. Fertilizer is not typically applied in  
490 West Africa until the start of the growing season—often April—but we find that much of  
491 the NH<sub>3</sub> increase occurs during February and March, suggesting that increasing fertilizer  
492 use is unlikely to provide a complete explanation for the NH<sub>3</sub> trend. Agriculture may  
493 nevertheless play a role, with enhanced burned area and especially CO concentrations in  
494 February suggestive of increased burning of crop stubble in preparation for planting during  
495 this time of year. Fires in this region tend to emit a greater proportion of less oxidized  
496 species such as NH<sub>3</sub> at the end of the dry season, consistent with a biomass burning source  
497 for the increasing NH<sub>3</sub> VCDs.

498 Decreases in NH<sub>3</sub> VCDs were largest in South Sudan, especially over the Sudd  
499 wetland, where NH<sub>3</sub> VCDs vary seasonally with the extent of area flooded. As the  
500 temporarily flooded areas of the Sudd dry out each year, NH<sub>3</sub> VCDs increase as reduction in  
501 soil moisture drives increased production and volatilization of NH<sub>3</sub>. The area of the Sudd  
502 that is flooded each year varies, and from 2008 until 2015, the area that remains flooded

503 during the dry season generally increased, producing a positive overall trend for the period  
504 of 2008 through 2017. This increase in the dry season flooded area drove a decrease in  
505  $\text{NH}_3$  VCDs: with less soil drying out, the seasonal maxima in  $\text{NH}_3$  VCDs were lower.  
506 Although it is possible that conflict in South Sudan could contribute to changes in  $\text{NH}_3$   
507 VCDs, the timing and distribution of conflict events and human displacement suggest that  
508 other factors are likely more important.

509 Modest increases in  $\text{NH}_3$  VCDs were observed in the Lake Victoria region. This  
510 region has experienced increases in agricultural area during the IASI observation period,  
511 and these changes explained a large proportion of the variation in  $\text{NH}_3$  VCDs across large  
512 patches of the region, where biomass burning could not. We expect that both expansion  
513 and intensification of agriculture in this region could contribute to the positive  $\text{NH}_3$  trend.

514 Considering national-scale statistics, comparisons between equally sized bins of 17  
515 countries each suggested that changes in biomass burning emissions and livestock  
516 emissions could contribute to differences in  $\text{NH}_3$  VCDs among countries, but variables  
517 related to cropped agriculture such as cropped area or fertilizer N use did not appear to be  
518 important factors at this scale. This may be because although fertilizer use has been  
519 increasing in sub-Saharan Africa, it remains extremely low relative to other continents, and  
520 relative to the levels needed to attain food security. Average fertilizer use in most  
521 countries in the region is under  $20 \text{ kg N ha}^{-1} \text{ yr}^{-1}$ , and sometimes less than  $5 \text{ kg N ha}^{-1} \text{ yr}^{-1}$ .  
522 Although recommended fertilizer rates are lower in most African countries than in the U.S.  
523 or Europe, increasing N inputs to 50 or  $100 \text{ kg N ha}^{-1} \text{ yr}^{-1}$  would represent a major  
524 perturbation to the regional N cycle, and potentially a large new source of  $\text{NH}_3$  to the  
525 atmosphere. West Africa is already a global  $\text{NH}_3$  hotspot (Van Damme et al., 2018),  
526 suggesting that encouraging policies that can help to limit  $\text{NH}_3$  emissions during the early  
527 stages of agricultural intensification in Africa may help mitigate potential impacts on the  
528 atmosphere. Fortunately, agricultural practices such as sub-surface application of  
529 fertilizer, which is already being promoted to smallholder farmers, can serve to both limit  
530  $\text{NH}_3$  emissions also help to increase crop yields.

531 These past and anticipated future trends also make the case for expanding capacity  
532 for atmospheric monitoring in sub-Saharan Africa. Although long-term monitoring  
533 networks have been established in West Africa (Adon et al., 2010; Ossouhou et al., 2019) and

534 South Africa (Conradie et al., 2016) as part of the INDAAF network, it is mainly focused on  
535 deposition and the spatio-temporal resolution of surface measurements is very coarse  
536 when compared to the data available in other parts of the world, which will limit our ability  
537 to understand how agricultural and socio-economic development in Africa affect the  
538 atmosphere. Satellite observations can help to bridge some of these data gaps, but have  
539 their own spatio-temporal limitations, and would further benefit from additional high-  
540 quality surface observations for evaluation of retrieval products.

541

542 **Data availability:** All data used in this study are available from public sources, with the  
543 exception of Sudd wetland extent, which is available by request from Courtney Di Vittorio. The  
544 IASI NH<sub>3</sub> and CO data are available from The IASI <https://iasi.aeris-data.fr>. The NOAA Global  
545 Surface Temperature Dataset is available at [https://data.nodc.noaa.gov/cgi-](https://data.nodc.noaa.gov/cgi-bin/iso?id=gov.noaa.ncdc:C01585)  
546 [bin/iso?id=gov.noaa.ncdc:C01585](https://data.nodc.noaa.gov/cgi-bin/iso?id=gov.noaa.ncdc:C01585). MODIS burned area data are available from  
547 <https://www.globalfiredata.org/data.html>. MODIS agricultural area are available at  
548 <https://lpdaac.usgs.gov/products/mcd12c1v006/>. TRMM 3B42 precipitation data are available  
549 from <https://pmm.nasa.gov/data-access/downloads/trmm>. The Gridded Livestock of the World  
550 data are available from <https://livestock.geo-wiki.org/home-2/>. Population density data for 2017  
551 are available at <https://landscan.ornl.gov/downloads/2017>. FAO national crop production and  
552 fertilizer N data are available at <http://www.fao.org/faostat/en/>. Data on conflict events from  
553 ACLED are available at <https://acleddata.com/#/dashboard>. World Bank national statistics  
554 on refugees and internally displaced people are available at <https://data.worldbank.org>.

555

556 **Author Contribution:** J.E.H. designed the study, conducted the analysis, and wrote the paper.  
557 NA, ED, CD, MO, CG-L, KT, and SEB contributed to study design and edited the paper. LC, P-  
558 FC, and MVD developed the original IASI trace gas retrievals and edited the paper.

559 The authors declare that they have no conflict of interest.

560

561 **Acknowledgements:** J.E.H.'s research was supported by an appointment to the NASA  
562 Postdoctoral Program at the NASA Goddard Institute for Space Studies administered by  
563 Universities Space Research Association under contract with NASA.

564

565

## 566 **References**

567 van der A, R. J., Eskes, H. J., Boersma, K. F., van Noije, T. P. C., Van Roozendaal, M., De Smedt,  
568 I., Peters, D. H. M. U. and Meijer, E. W.: Trends, seasonal variability and dominant NO<sub>x</sub>  
569 source derived from a ten year record of NO<sub>2</sub> measured from space, *J. Geophys. Res.*  
570 *Atmos.*, 113(4), D04302, doi:10.1029/2007JD009021, 2008.

571 Adon, M., Galy-Lacaux, C., Yoboué, V., Delon, C., Lacaux, J. P., Castera, P., Gardrat, E., Pienaar,  
572 J., Al Ourabi, H., Laouali, D., Diop, B., Sigha-Nkamdjou, L., Akpo, a., Tathy, J. P., Lavenu, F. and  
573 Mougin, E.: Long term measurements of sulfur dioxide, nitrogen dioxide, ammonia, nitric  
574 acid and ozone in Africa using passive samplers, *Atmos. Chem. Phys.*, 10(15), 7467–7487,  
575 doi:10.5194/acp-10-7467-2010, 2010.

576 AGRA: AGRA in 2008: Building on the New Momentum in African Agriculture., 2009.

577 Andela, N. and van der Werf, G. R.: Recent trends in African fires driven by cropland  
578 expansion and El Niño to la Niña transition, *Nat. Clim. Chang.*, 4(9), 791–795,  
579 doi:10.1038/nclimate2313, 2014.

580 Andela, N., Morton, D. C., Giglio, L., Chen, Y., Van Der Werf, G. R., Kasibhatla, P. S., DeFries, R.  
581 S., Collatz, G. J., Hantson, S., Kloster, S., Bachelet, D., Forrest, M., Lasslop, G., Li, F., Mangeon,  
582 S., Melton, J. R., Yue, C. and Randerson, J. T.: A human-driven decline in global burned area,  
583 *Science* (80-. ), 356(6345), 1356–1362, doi:10.1126/science.aal4108, 2017.

584 Anker, H. T., Baaner, L., Backes, C., Keessen, A. and Möckel, S.: Comparison of ammonia  
585 regulation in Germany , the Netherlands and Denmark – legal framework, Copenhagen,  
586 2018.

587 Bauer, S. E., Tsigaridis, K. and Miller, R.: Significant atmospheric aerosol pollution caused by  
588 world food cultivation, *Geophys. Res. Lett.*, 43(10), 5394–5400,  
589 doi:10.1002/2016GL068354, 2016.

590 Behera, S. N., Sharma, M., Aneja, V. P. and Balasubramanian, R.: Ammonia in the  
591 atmosphere: A review on emission sources, atmospheric chemistry and deposition on

592 terrestrial bodies, *Environ. Sci. Pollut. Res.*, 20(11), 8092–8131, doi:10.1007/s11356-013-  
593 2051-9, 2013.

594 Bouwman, A. F., Lee, D. S., Asman, W. A. H., Dentener, F. J., Van Der Hoek, K. W. and Olivier, J.  
595 G. J.: A global high-resolution emission inventory for ammonia, *Global Biogeochem. Cycles*,  
596 11(4), 561–587, 1997.

597 Bustamante, M. M. C., Medina, E., Asner, G. P., Nardoto, G. B. and Garcia-Montiel, D. C.:  
598 Nitrogen cycling in tropical and temperate savannas, *Biogeochemistry*, 79(1–2), 209–237,  
599 doi:10.1007/s10533-006-9006-x, 2006.

600 Cahoon, D. R., Stocks, B. J., Levine, J. S., Cofer, W. R. and O'Neill, K. P.: Seasonal distribution of  
601 African savanna fires, *Nature*, 359(6398), 812–815, doi:10.1038/359812a0, 1992.

602 Chen, L.-W. A., Verburg, P., Shackelford, A., Zhu, D., Susfalk, R., Chow, J. C. and Watson, J. G.:  
603 Moisture effects on carbon and nitrogen emission from burning of wildland biomass,  
604 *Atmos. Chem. Phys.*, 10(14), 6617–6625, doi:10.5194/acp-10-6617-2010, 2010.

605 Chilonda, P. and Otte, J.: Indicators to monitor trends in livestock production at national,  
606 regional and international levels, *Livest. Res. Rural Dev.*, 18(8), 1–12, 2006.

607 Clarisse, L., Clerbaux, C., Dentener, F., Hurtmans, D. and Coheur, P. F.: Global ammonia  
608 distribution derived from infrared satellite observations, *Nat. Geosci.*, 2(7), 479–483,  
609 doi:10.1038/ngeo551, 2009.

610 Clarisse, L., Van Damme, M., Gardner, W., Coheur, P.-F., Clerbaux, C., Whitburn, S., Hadji-  
611 Lazaro, J. and Hurtmans, D.: Atmospheric ammonia (NH<sub>3</sub>) emanations from Lake Natron's  
612 saline mudflats, *Sci. Rep.*, 9, 4441, doi:10.1038/s41598-019-39935-3, 2019.

613 Cobo, J. G., Dercon, G. and Cadisch, G.: Nutrient balances in African land use systems across  
614 different spatial scales: A review of approaches, challenges and progress, *Agric. Ecosyst.*  
615 *Environ.*, 136(1–2), 1–15, doi:10.1016/j.agee.2009.11.006, 2010.

616 Conradie, E. H., Van Zyl, P. G., Pienaar, J. J., Beukes, J. P., Galy-Lacaux, C., Venter, A. D. and  
617 Mkhathshwa, G. V.: The chemical composition and fluxes of atmospheric wet deposition at  
618 four sites in South Africa, *Atmos. Environ.*, 146, 113–131,  
619 doi:10.1016/j.atmosenv.2016.07.033, 2016.

620 Van Damme, M., Wichink Kruit, R. J., Schaap, M., Clarisse, L., Clerbaux, C., Coheur, P. F.,  
621 Dammers, E., Dolman, A. J. and Erisman, J. W.: Evaluating 4 years of atmospheric ammonia  
622 (NH<sub>3</sub>) over Europe using IASI satellite observations and LOTOS-EUROS model results, J.

623 Geophys. Res., 119(15), 9549–9566, doi:10.1002/2014JD021911, 2014a.

624 Van Damme, M., Clarisse, L., Heald, C. L., Hurtmans, D., Ngadi, Y., Clerbaux, C., Dolman, A. J.,  
625 Erisman, J. W. and Coheur, P. F.: Global distributions, time series and error characterization  
626 of atmospheric ammonia NH<sub>3</sub> from IASI satellite observations, *Atmos. Chem. Phys.*, 14(6),  
627 2905–2922, doi:10.5194/acp-14-2905-2014, 2014b.

628 Van Damme, M., Clarisse, L., Dammers, E., Liu, X., Nowak, J. B., Clerbaux, C., Flechard, C. R.,  
629 Galy-Lacaux, C., Xu, W., Neuman, J. A., Tang, Y. S., Sutton, M. A., Erisman, J. W. and Coheur, P.  
630 F.: Towards validation of ammonia (NH<sub>3</sub>) measurements from the IASI satellite, *Atmos.*  
631 *Meas. Tech.*, 8(3), 1575–1591, doi:10.5194/amt-8-1575-2015, 2015.

632 Van Damme, M., Whitburn, S., Clarisse, L., Clerbaux, C., Hurtmans, D. and Coheur, P. F.:  
633 Version 2 of the IASI NH<sub>3</sub> neural network retrieval algorithm: Near-real-time and  
634 reanalysed datasets, *Atmos. Meas. Tech.*, 10(12), 4905–4914, doi:10.5194/amt-10-4905-  
635 2017, 2017.

636 Van Damme, M., Clarisse, L., Whitburn, S., Hadji-Lazaro, J., Hurtmans, D., Clerbaux, C. and  
637 Coheur, P.: Industrial and agricultural ammonia point sources exposed, *Nature*, 564, 99–  
638 103, 2018.

639 Van Damme, M., Clarisse, L., Franco, B., Sutton, M. A., Erisman, J. W., Wichink Kruit, R., van  
640 Zanten, M., Whitburn, S., Hadji-Lazaro, J., Hurtmans, D., Clerbaux, C. and Coheur, P.-F.:  
641 Global, regional and national trends of atmospheric ammonia derived from a decadal  
642 (2008-2018) satellite record, *Environ. Res. Lett.*, 16, 055017, 2021.

643 Dammers, E., Palm, M., Van Damme, M., Vigouroux, C., Smale, D., Conway, S., Toon, G. C.,  
644 Jones, N., Nussbaumer, E., Warneke, T., Petri, C., Clarisse, L., Clerbaux, C., Hermans, C.,  
645 Lutsch, E., Strong, K., Hannigan, J. W., Nakajima, H., Morino, I., Herrera, B., Stremme, W.,  
646 Grutter, M., Schaap, M., Kruit, R. J. W., Notholt, J., Coheur, P. F. and Erisman, J. W.: An  
647 evaluation of IASI-NH<sub>3</sub> with ground-based Fourier transform infrared spectroscopy  
648 measurements, *Atmos. Chem. Phys.*, 16(16), 10351–10368, doi:10.5194/acp-16-10351-  
649 2016, 2016.

650 Denier Van Der Gon, H. and Bleeker, A.: Indirect N<sub>2</sub>O emission due to atmospheric N  
651 deposition for the Netherlands, *Atmos. Environ.*, 39(32), 5827–5838,  
652 doi:10.1016/j.atmosenv.2005.06.019, 2005.

653 Dobson, J. E., Bright, E. A., Coleman, P. R., Durfee, R. C. and Worley, B. A.: A global population

654 database for estimating populations at risk, *Photogramm. Eng. Remote Sens.*, 66(7), 849–  
655 857, 2000.

656 Doumbia, E. H. T., Liousse, C., Keita, S., Granier, L., Granier, C., Elvidge, C. D., Elguindi, N. and  
657 Law, K.: Flaring emissions in Africa: Distribution, evolution and comparison with current  
658 inventories, *Atmos. Environ.*, 199, 423–434, doi:10.1016/j.atmosenv.2018.11.006, 2019.

659 Elrys, A. S., Abdel-Fattah, M. K., Raza, S., Chen, Z. and Zhou, J.: Spatial trends in the nitrogen  
660 budget of the African agro-food system over the past five decades, *Environ. Res. Lett.*,  
661 14(12), doi:10.1088/1748-9326/ab5d9e, 2019.

662 European Commission Joint Research Centre (JRC)/Netherlands Environmental  
663 Assessment Agency (PBL): Emission Database for Global Atmospheric Research (EDGAR),  
664 release version 4.3.1, 2016.

665 Fan, Y. and van den Dool, H.: A global monthly land surface air temperature analysis for  
666 1948-present, *J. Geophys. Res. Atmos.*, 113(1), D01103, doi:10.1029/2007JD008470, 2008.

667 FAO: FAO Statistics Database, FAOSTAT Stat. Database [online] Available from:  
668 <http://www.fao.org/faostat/en/> (Accessed 1 January 2020), 2020.

669 Friedl, M. A., McIver, D. K., Hodges, J. C. F., Zhang, X. Y., Muchoney, D., Strahler, A. H.,  
670 Woodcock, C. E., Gopal, S., Schneider, A., Cooper, A., Baccini, A., Gao, F. and Schaaf, C.: Global  
671 land cover mapping from MODIS: Algorithms and early results, *Remote Sens. Environ.*,  
672 83(1–2), 287–302, doi:10.1016/S0034-4257(02)00078-0, 2002.

673 Galy-Lacaux, C. and Delon, C.: Nitrogen emission and deposition budget in West and Central  
674 Africa, *Environ. Res. Lett.*, 9(12), doi:10.1088/1748-9326/9/12/125002, 2014.

675 Gbadegesin, A. and Olusesi, B. B.: Effects of land clearing methods on soil physical and  
676 hydrological properties in southwestern Nigeria, *Environmentalist*, 14(4), 297–303, 1994.

677 George, M., Clerbaux, C., Hurtmans, D., Turquety, S., Coheur, P. F., Pommier, M., Hadji-  
678 Lazaro, J., Edwards, D. P., Worden, H., Luo, M., Rinsland, C. and McMillan, W.: Carbon  
679 monoxide distributions from the IASI/METOP mission: Evaluation with other space-borne  
680 remote sensors, *Atmos. Chem. Phys.*, 9(21), 8317–8330, doi:10.5194/acp-9-8317-2009,  
681 2009.

682 Giglio, L., Boschetti, L., Roy, D. P., Humber, M. L. and Justice, C. O.: The Collection 6 MODIS  
683 burned area mapping algorithm and product, *Remote Sens. Environ.*, 217, 72–85,  
684 doi:10.1016/j.rse.2018.08.005, 2018.

685 Global Internal Displacement Monitoring Centre: Global Internal Displacement Database,  
686 [online] Available from: <https://www.internal-displacement.org/database/displacement->  
687 [data](https://www.internal-displacement.org/database/displacement-data), 2020.

688 Goode, J. G., Yokelson, R. J., Susott, R. A. and Ward, D. E.: Trace gas emissions from  
689 laboratory biomass fires measured by open-path Fourier transform infrared spectroscopy.,  
690 *J. Chem. Inf. Model.*, 104(D17), 21237–21245, 1999.

691 Guo, X., Clarisse, L., Wang, R., Van Damme, M., Whitburn, S., Coheur, P., Clerbaux, C., Franco,  
692 B., Pan, D., Golston, L. M., Wendt, L., Sun, K., Tao, L., Miller, D., Mikoviny, T., Müller, M.,  
693 Wisthaler, A., Tevlin, A. G., Murphy, J. G., Nowak, J. B., Roscioli, J. R., Volkamer, R., Kille, N.,  
694 Neuman, J. A., Eilerman, S. J., Crawford, J. H., Yacovitch, T. I., Barrick, J. D., Scarino, A. J. and  
695 Zondlo, M. A.: Validation of IASI satellite ammonia observations at the pixel scale using in-  
696 situ vertical profiles, *J. Geophys. Res. Atmos.*, 126, e2020JD033475,  
697 doi:10.1029/2020jd033475, 2021.

698 Hazell, P. and Wood, S.: Drivers of change in global agriculture., *Philos. Trans. R. Soc. Lond.*  
699 *B. Biol. Sci.*, 363(1491), 495–515, doi:10.1098/rstb.2007.2166, 2008.

700 Hickman, J. E., Dammers, E., Galy-Lacaux, C. and Van Der Werf, G. R.: Satellite evidence of  
701 substantial rain-induced soil emissions of ammonia across the Sahel, *Atmos. Chem. Phys.*,  
702 18(22), 16713–16727, doi:10.5194/acp-18-16713-2018, 2018.

703 Hickman, J. E., Andela, N., Tsigaridis, K., Galy-Lacaux, C., Osohou, M. and Bauer, S. E.:  
704 Reductions in NO<sub>2</sub> burden over north equatorial Africa from decline in biomass burning in  
705 spite of growing fossil fuel use, 2005 to 2017 , *Proc. Natl. Acad. Sci.*, 118(7), e2002579118,  
706 doi:10.1073/pnas.2002579118, 2021a.

707 Hickman, J. E., Dammers, E., Galy-Lacaux, C., Osohou, M. and Bauer, S. E.: Continental and  
708 ecoregion-specific drivers of atmospheric NO<sub>2</sub> and NH<sub>3</sub> seasonality over Africa revealed by  
709 satellite observations, *Global Biogeochem. Cycles*, 35, e2020GB006916,  
710 doi:10.1029/2020GB006916, 2021b.

711 Huffman, G. J., Adler, R. F., Bolvin, D. T., Gu, G., Nelkin, E. J., Bowman, K. P., Hong, Y., Stocker,  
712 E. F. and Wolff, D. B.: The TRMM Multisatellite Precipitation Analysis (TMPA): Quasi-Global,  
713 Multiyear, Combined-Sensor Precipitation Estimates at Fine Scales, *J. Hydrometeorol.*, 8(1),  
714 38–55, doi:10.1175/jhm560.1, 2007.

715 Hurtmans, D., Coheur, P. F., Wespes, C., Clarisse, L., Scharf, O., Clerbaux, C., Hadji-Lazaro, J.,



716 George, M. and Turquety, S.: FORLI radiative transfer and retrieval code for IASI, *J. Quant.*  
717 *Spectrosc. Radiat. Transf.*, 113(11), 1391–1408, doi:10.1016/j.jqsrt.2012.02.036, 2012.

718 Idris, I.: *Livestock and conflict in South Sudan - K4D Helpdesk Report 484*, Brighton, 2018.

719 Kanter, D. R.: Nitrogen pollution: a key building block for addressing climate change, *Clim.*  
720 *Change*, 147(1–2), 11–21, doi:10.1007/s10584-017-2126-6, 2018.

721 Kerzenmacher, T., Dils, B., Kumps, N., Blumenstock, T., Clerbaux, C., Coheur, P. F., Demoulin,  
722 P., García, O., George, M., Griffith, D. W. T., Hase, F., Hadji-Lazaro, J., Hurtmans, D., Jones, N.,  
723 Mahieu, E., Notholt, J., Paton-Walsh, C., Raffalski, U., Ridder, T., Schneider, M., Servais, C. and  
724 De Mazière, M.: Validation of IASI FORLI carbon monoxide retrievals using FTIR data from  
725 NDACC, *Atmos. Meas. Tech.*, 5(11), 2751–2761, doi:10.5194/amt-5-2751-2012, 2012.

726 Korontzi, S., McCarty, J., Loboda, T., Kumar, S. and Justice, C.: Global distribution of  
727 agricultural fires in croplands from 3 years of Moderate Resolution Imaging  
728 Spectroradiometer (MODIS) data, *Global Biogeochem. Cycles*, 20(2), GB2021,  
729 doi:10.1029/2005GB002529, 2006.

730 Krupa, S. V.: Effects of atmospheric ammonia (NH<sub>3</sub>) on terrestrial vegetation: A review,  
731 *Environ. Pollut.*, 124(2), 179–221, doi:10.1016/S0269-7491(02)00434-7, 2003.

732 Lee, C., Martin, R. V., Van Donkelaar, A., Lee, H., Dickerson, R. R., Hains, J. C., Krotkov, N.,  
733 Richter, A., Vinnikov, K. and Schwab, J. J.: SO<sub>2</sub> emissions and lifetimes: Estimates from  
734 inverse modeling using in situ and global, space-based (SCIAMACHY and OMI)  
735 observations, *J. Geophys. Res. Atmos.*, 116(6), 1–13, doi:10.1029/2010JD014758, 2011.

736 Lelieveld, J., Evans, J. S., Fnais, M., Giannadaki, D. and Pozzer, A.: The contribution of outdoor  
737 air pollution sources to premature mortality on a global scale, *Nature*, 525(7569), 367–371,  
738 doi:10.1038/nature15371, 2015.

739 Masso, C., Nziguheba, G., Mtutegi, J., Galy-Lacaux, C., Wendt, K., Butterbach-Bahl, K., Wairegi,  
740 L. and Datta, A.: Soil fertility Management in Sub-Saharan Africa, in *Sustainable Agriculture*  
741 *Reviews*, edited by E. Lichtfouse, p. 304, Springer International Publishing., 2017.

742 Nicholson, S., Some, B., McCollum, J., Nelkin, E., Klotter, D., Berte, Y., Diallo, B., Gaye, I.,  
743 Kpabeba, G., Ndiaye, O., Noukpozoukou, J., Tanu, M., Thiam, A., Toure, A. and Traore, A.:  
744 Validation of TRMM and other rainfall estimates with a high-density gauge dataset for West  
745 Africa. Part II: Validation of TRMM rainfall products, *J. Appl. Meteorol.*, 42, 1355–1368,  
746 2003.

747 Ossohou, M., Galy-Lacaux, C., Yoboué, V., Hickman, J. E., Gardrat, E., Adon, M., Darras, S.,  
748 Laouali, D., Akpo, A., Ouafo, M., Diop, B. and Opepa, C.: Trends and seasonal variability of  
749 atmospheric NO<sub>2</sub> and HNO<sub>3</sub> concentrations across three major African biomes inferred  
750 from long-term series of ground-based and satellite measurements, *Atmos. Environ.*, 207,  
751 148–166, 2019.

752 Pamela A. Matson, McDowell, W. H., Townsend, A. R. and Vitousek, P. M.: The globalization  
753 of N deposition: ecosystem consequences in tropical environments, *Biogeochemistry*, 46,  
754 67–83, 1999.

755 Pommier, M., Law, K. S., Clerbaux, C., Turquety, S., Hurtmans, D., Hadji-Lazaro, J., Coheur, P.  
756 F., Schlager, H., Ancellet, G., Paris, J. D., Nédélec, P., Diskin, G. S., Podolske, J. R., Holloway, J. S.  
757 and Bernath, P.: IASI carbon monoxide validation over the Arctic during POLARCAT spring  
758 and summer campaigns, *Atmos. Chem. Phys.*, 10(21), 10655–10678, doi:10.5194/acp-10-  
759 10655-2010, 2010.

760 Pope, A., Burnett, R., Thun, M., EE, C., D, K., I, K. and GD, T.: Long-term Exposure to Fine  
761 Particulate Air Pollution, *J. Am. Med. Assoc.*, 287(9), 1132–1141,  
762 doi:10.1001/jama.287.9.1132, 2002.

763 Raleigh, C., Linke, A., Hegre, H. and Karlsen, J.: Introducing ACLED: An Armed Conflict  
764 Location and Event Dataset: Special Data Feature, *J. Peace Res.*, 47(5), 651–660,  
765 doi:https://doi.org/10.1177/0022343310378914, 2010.

766 Ramo, R., Roteta, E., Bistinas, I., van Wees, D., Bastarrika, A., Chuvieco, E. and van der Werf,  
767 G. R.: African burned area and fire carbon emissions are strongly impacted by small fires  
768 undetected by coarse resolution satellite data, *Proc. Natl. Acad. Sci. U. S. A.*, 118(9), 1–7,  
769 doi:10.1073/pnas.2011160118, 2021.

770 Robinson, T. P., Wint, G. R. W., Conchedda, G., Van Boeckel, T. P., Ercoli, V., Palamara, E.,  
771 Cinardi, G., D’Aietti, L., Hay, S. I. and Gilbert, M.: Mapping the Global Distribution of  
772 Livestock, *PLoS One*, 9(5), e96084, doi:10.1371/journal.pone.0096084, 2014.

773 Roteta, E., Bastarrika, A., Padilla, M., Storm, T. and Chuvieco, E.: Development of a Sentinel-2  
774 burned area algorithm: Generation of a small fire database for sub-Saharan Africa, *Remote  
775 Sens. Environ.*, 222(November 2018), 1–17, doi:10.1016/j.rse.2018.12.011, 2019.

776 Rufino, M. C., Rowe, E. C., Delve, R. J. and Giller, K. E.: Nitrogen cycling efficiencies through  
777 resource-poor African crop-livestock systems, *Agric. Ecosyst. Environ.*, 112(4), 261–282,

778 doi:10.1016/j.agee.2005.08.028, 2006.

779 Sauvage, B., Gheusi, F., Thouret, V., Cammas, J. P., Duron, J., Escobar, J., Mari, C., Mascart, P.  
780 and Pont, V.: Medium-range mid-tropospheric transport of ozone and precursors over  
781 Africa: Two numerical case studies in dry and wet seasons, *Atmos. Chem. Phys.*, 7(20),  
782 5357–5370, doi:10.5194/acp-7-5357-2007, 2007.

783 Stevens, C. J., David, T. I. and Storkey, J.: Atmospheric nitrogen deposition in terrestrial  
784 ecosystems: Its impact on plant communities and consequences across trophic levels,  
785 *Funct. Ecol.*, 32(7), 1757–1769, doi:10.1111/1365-2435.13063, 2018.

786 Sutton, M. A., Reis, S., Riddick, S. N., Dragosits, U., Nemitz, E., Theobald, M. R., Tang, Y. S.,  
787 Braban, C. F., Vieno, M., Dore, A. J., Mitchell, R. F., Wanless, S., Daunt, F., Fowler, D., Blackall,  
788 T. D., Milford, C., Flechard, C. R., Loubet, B., Massad, R., Cellier, P., Personne, E., Coheur, P. F.,  
789 Clarisse, L., Van Damme, M., Ngadi, Y., Clerbaux, C., Skøth, C. A., Geels, C., Hertel, O., Wichink  
790 Kruit, R. J., Pinder, R. W., Bash, J. O., Walker, J. T., Simpson, D., Horváth, L., Misselbrook, T. H.,  
791 Bleeker, A., Dentener, F. and de Vries, W.: Towards a climate-dependent paradigm of  
792 ammonia emission and deposition, *Philos. Trans. R. Soc. B Biol. Sci.*, 368(1621), 20130166–  
793 20130166, doi:10.1098/rstb.2013.0166, 2013.

794 Tian, D. and Niu, S.: A global analysis of soil acidification caused by nitrogen addition,  
795 *Environ. Res. Lett.*, 10(2), 024019, doi:10.1088/1748-9326/10/2/024019, 2015.

796 USDA Agricultural Air Quality Task Force: Ammonia Emissions : What To Know Before You  
797 Regulate, Washington, DC. [online] Available from:  
798 <http://www.nrcs.usda.gov/wps/portal/nrcs/detail/national/air/taskforce/?cid=stelprdb1>  
799 268645, 2014.

800 Vitousek, P., Naylor, R., Crews, T., David, M., Drinkwater, L., Holland, E., Johnes, P.,  
801 Katzenberger, J., Martinelli, L. A., Matson, P. A., Nziguheba, G., Ojima, D., Palm, C. A.,  
802 Robertson, G., Sanchez, P., Townsend, A. and Zhang, F.: Nutrient Imbalances in Agricultural  
803 Development, *Science*, 324, 1519–1520, 2009.

804 Di Vittorio, C. A. and Georgakakos, A. P.: Land cover classification and wetland inundation  
805 mapping using MODIS, *Remote Sens. Environ.*, 204, 1–17, doi:10.1016/j.rse.2017.11.001,  
806 2018.

807 Vrieling, A., de Beurs, K. M. and Brown, M. E.: Variability of African farming systems from  
808 phenological analysis of NDVI time series, *Clim. Change*, 109(3–4), 455–477,

809 doi:10.1007/s10584-011-0049-1, 2011.

810 De Wachter, E., Barret, B., Le Flochmoën, E., Pavelin, E., Matricardi, M., Clerbaux, C., Hadji-  
811 Lazaro, J., George, M., Hurtmans, D., Coheur, P. F., Nedelec, P. and Cammas, J. P.: Retrieval of  
812 MetOp-A/IASI CO profiles and validation with MOZAIC data, *Atmos. Meas. Tech.*, 5(11),  
813 2843–2857, doi:10.5194/amt-5-2843-2012, 2012.

814 Warner, J. X., Dickerson, R. R., Wei, Z., Strow, L. L., Wang, Y. and Liang, Q.: Increased  
815 atmospheric ammonia over the world’s major agricultural areas detected from space,  
816 *Geophys. Res. Lett.*, 44(6), 2875–2884, doi:10.1002/2016GL072305, 2017.

817 Whitburn, S., Van Damme, M., Kaiser, J. W., Van Der Werf, G. R., Turquety, S., Hurtmans, D.,  
818 Clarisse, L., Clerbaux, C. and Coheur, P. F.: Ammonia emissions in tropical biomass burning  
819 regions: Comparison between satellite-derived emissions and bottom-up fire inventories,  
820 *Atmos. Environ.*, 121, 42–54, doi:10.1016/j.atmosenv.2015.03.015, 2015.

821 World Bank: World Bank Open Data, World Bank Open Data [online] Available from:  
822 <https://www.data.worldbank.org> (Accessed 2 February 2019), 2019

823 Yegbemey, R. N., Kabir, H., Awoye, O. H. R., Yabi, J. A. and Paraiso, A. A.: Managing the  
824 agricultural calendar as coping mechanism to climate variability: A case study of maize  
825 farming in northern Benin, West Africa, *Clim. Risk Manag.*, 3, 13–23,  
826 doi:10.1016/j.crm.2014.04.001, 2014.

827 Yokelson, R. J., Christian, T. J., Karl, T. G. and Guenther, A.: The tropical forest and fire  
828 emissions experiment: laboratory fire measurements and synthesis of campaign, *Rev. Int.*  
829 *Acupunt.*, 8, 3509–3527, doi:10.1016/s1887-8369(09)71579-0, 2008.

830 Zheng, B., Chevallier, F., Ciais, P., Yin, Y. and Wang, Y.: On the Role of the Flaming to  
831 Smoldering Transition in the Seasonal Cycle of African Fire Emissions, *Geophys. Res. Lett.*,  
832 45(21), 11,998-12,007, doi:10.1029/2018GL079092, 2018.

833

834 **Figure 1.** Annual averages and trends in atmospheric NH<sub>3</sub> VCDs, CO VCDs, and  
835 burned area, as well as spatial distribution of livestock density and cropped area across  
836 seven sub-Saharan African ecoregions. Mean annual (a) and trend (b) in atmospheric NH<sub>3</sub>  
837 VCDs from IASI for the period 2008 through 2018. Mean annual (c) and trend (d) in annual  
838 atmospheric CO VCDs from IASI for the same period. Mean annual (e) and trend (f) in  
839 annual burned area from MODIS for 2008-2018. Livestock densities for 2007 from the FAO

840 (f), and mean cropped area from MODIS for 2008-2018 (g). The border of South Sudan is  
841 highlighted in black, and several regions boxed: the Nile region at 30°N, the Sudd wetland  
842 in South Sudan, the Lake Victoria region at the equator, and West Africa centered around  
843 10°N.

844  
845 **Figure 2.** Relationships between NH<sub>3</sub> trends and livestock density, population  
846 density, and cropland area, as well as changes in cropland area. Spatial correlations  
847 between changes in annual atmospheric NH<sub>3</sub> VCDs and livestock density (a) and population  
848 density (b). Correlation between cropland area and NH<sub>3</sub> VCDs for 2008 through 2018 (c).  
849 Change in crop area for 2008 through 2018 (d). The NH<sub>3</sub> and crop area trends are based on  
850 data for 2008 through 2018, livestock density data are for the year 2007, population  
851 density data are for the year 2017.

852  
853 **Figure 3.** Change in mean monthly atmospheric NH<sub>3</sub> VCDs for the period 2008  
854 through 2018. Grid cells where mean annual NH<sub>3</sub> VCDs for the entire period are under  
855  $5 \times 10^{15}$  molecules cm<sup>-2</sup> are not displayed. Results significant at P=0.05 are presented in  
856 Figure S5.

857 **Figure 4.** Correlation coefficient for the relationship between mean annual CO and  
858 NH<sub>3</sub> VCDs (a), changes in NH<sub>3</sub> VCDs (b) and changes in CO VCDs (c) over 2008 through  
859 2018 in West Africa. Grid cells where mean annual NH<sub>3</sub> VCDs for the entire period are  
860 under  $5 \times 10^{15}$  molecules cm<sup>-2</sup> are not displayed. Results significant at P=0.05 for the entire  
861 continent are presented in Figure S6.

862 **Figure 5.** Mean (a) monthly and (b) February through May annual mean flooded  
863 extent of the Sudd, surface temperatures over South Sudan, and NH<sub>3</sub> VCDs over the Sudd  
864 and the entirety of South Sudan for the period 2008 through 2017.

865 **Figure 6. Changes in NH<sub>3</sub> VCDs and their relationship with burned area and**  
866 **cropped area** over the Lake Victoria region for the 2008 through 2018 period. (a)  
867 Correlation coefficients for the relationship between NH<sub>3</sub> VCDs and burned area. (b)

868 Correlation coefficients for the relationship between NH<sub>3</sub> VCDs and cropped area, including  
869 mosaics of crops and natural vegetation cover. (c) Changes in NH<sub>3</sub> VCDs.

870

871 **Figure 7.** Annual percentage changes in national mean annual NH<sub>3</sub> VCDs, burned  
872 area, CO VCDs, livestock, crop yield, and fertilizer N use for African countries with low,  
873 medium, or high rates of NH<sub>3</sub> VCD change. Error bars represent the standard error of the  
874 mean. See Table S1 for the list of countries in each bin and Fig. S19 for an expanded set of  
875 variables.

876

877